BOLETIN DE LA SOCIEDAD ESPAÑOLA DE
Cerámica y Vidrio
www.elsevier.es/bsecv

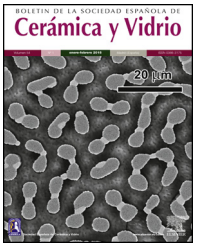

Fabrication and properties of novel porous ceramic membrane supports from the (Sig) diatomite and alumina mixtures

Fayçal Aouadja[a,b], *Ferhat Bouzerara*[a,c,*], *Cetin Meric Guvenc*[d], *Mustafa M. Demir*[d]

[a] *Faculty of Exact Science and Informatics, Physics Department, Laboratory of Condensed Matter Physics and Nanomaterials, Jijel University, Jijel 18000, Algeria*
[b] *Research Center in Industriel Technologies CRTI, P.O. Box 64, Cheraga Algiers, Algeria*
[c] *laboratoire d'Etudes des Matériaux, Jijel University, Jijel 18000, Algeria*
[d] *Department of Materials Science and Engineering, İzmir Institute of Technology, 35430 Gülbahçe, Urla, İzmir, Turkey*

ARTICLE INFO

Article history:
Received 1 March 2021
Accepted 13 April 2021
Available online 4 May 2021

Keywords:
Ceramic
Membrane supports
Porosity
Diatomite
Strength

ABSTRACT

In this paper, the manufacturing of macro-porous tubular ceramic supports for membranes is described. The novel supports are fabricated from natural diatomite and alumina raw materials using the extrusion method. The structure was analyzed by X-ray diffraction (XRD) and mercury porosimetry techniques; the presence of possible defects was investigated by scanning electron microscopy (SEM). The permeability has been measured from water flux in standard experiments. Experimental results show that the open porosity, the average pore size (APS), the pore size distribution, the strength, and the permeability of sintered supports, have been found to depend, mainly on the concentration of alumina (Al_2O_3) additive. Supports prepared with the addition of 10 wt.% of alumina and sintered at 1200 °C, can be considered as the most optimized; they have a porosity ratio of about 46%, an APS is around 7.7 μm, a flexural strength value of about 28 MPa, and water permeability of around 15 $m^3\,h^{-1}\,m^{-2}\,bar^{-1}$. Such materials could be of great interest in the supports fabrication for membrane application, for instance, water filtration.

Fabricación y propiedades de nuevos soportes de membranas cerámicas porosas a partir de mezclas de (Sig) diatomita y alúmina

Palabras clave:
Cerámica
Soportes de membrana
Porosidad
Diatomita
Fuerza

RESUMEN

En este trabajo se describe la fabricación de soportes cerámicos tubulares macroporosos para membranas. Los nuevos soportes se fabrican a partir de materias primas de diatomita natural y alúmina mediante el método de extrusión. La estructura se analizó por medio de técnicas de difracción de rayos X (XRD) y porosimetría de mercurio; la presencia de posibles defectos se investigó mediante microscopía electrónica de barrido (SEM). La permeabilidad se ha medido a partir del flujo de agua en experimentos estándar. Los resultados

* *Corresponding author.*
E-mail addresses: bouzerara.f@gmail.com, f.bouzerara@univ-jijel.dz (F. Bouzerara).
https://doi.org/10.1016/j.bsecv.2021.04.002

experimentales muestran que se ha encontrado que la porosidad abierta, el tamaño medio de poro (APS), la distribución del tamaño de poro, la resistencia y la permeabilidad de los soportes sinterizados dependen, principalmente, de la concentración de aditivo de alúmina (Al_2O_3). Los soportes preparados con la adición de 10% en peso de alúmina y sinterizados a 1.200 °C, pueden considerarse como los más optimizados; tienen una relación de porosidad de alrededor del 46%, un APS es de alrededor de 7,7 μm, un valor de resistencia a la flexión de alrededor de 28 MPa y una permeabilidad al agua de alrededor de 15 $m^3.h^{-1}.m^{-2}.bar^{-1}$. Dichos materiales podrían ser de gran interés en la fabricación de soportes para la aplicación de membranas, por ejemplo, filtración de agua.

Introduction

The valorization of natural ceramic materials for industrial applications, such as membrane technology, is of the utmost importance because of the obvious economic benefits [1]. Nowadays, under the combined effect of industrial competition and new constraints related to the protection of the environment, researchers are focusing on the development of new ceramic membranes based on raw materials at low costs [2,3].

Algeria is one of the world's countries with vast reserves of raw ceramic materials, such as calcite ($CaCO_3$), dolomite ($CaCO_3{\cdot}MgCO_3$), kaolin, quartz, and diatomite. Many studies have already been published on the valorization of these native raw materials in many areas of technology, such as thermal ceramics [4], advanced ceramics [5], and ceramic membranes [3,6,7].

Membranes can be made from different materials e.g., ceramics, polymers, metals and/or glasses [8–10]. Ceramic membranes are costly, compared to polymeric membranes; however, they have relatively good properties such as: thermal stability, chemical resistance, mechanical resistance, permeability and durability [11]. The high strength of the ceramic materials allows the use of high trans-membrane pressures. Chemical stability makes the utilization of chemically aggressive cleaning products safe; also, it serves as an appropriate solution in several separation processes and harsh environments. Furthermore, thermal stability ensures that such membranes are ideal for applications at high-temperatures. Moreover, ceramic membranes are less vulnerable to microbial attacks and biological degradations [12,13]. As a result, porous ceramic membranes have different industrial applications in areas such as microfiltration (MF), ultrafiltration (UF), nanofiltration (NF), for concentrating or separating several compounds from water or other liquids in diverse fields such as food, textile, pharmacy, chemicals or leather industries [14,15]. Ceramic membranes are also proposed for environmental and energy applications in treatment/separation processes of gas, steam, and water [16].

In recent years, considerable work has been done at the international level to improve the cost-effectiveness of membranes destined for water filtration. Most interest is devoted to developing membranes with good permeability, high selectivity, and good resistance at low prices [17]. Of course, there are limits when we try to minimize the cost of manufacturing supports utilizing high-purity ceramic materials, such as silicon carbide, mullite, zirconia, and pure alumina [18,19]. Membranes are mainly composed of a thin filtering layer and a porous support. The latter provides the needed mechanical strength for the thin separation layer. Many studies have been carried out, and several materials have been proposed, in support preparation, such as Al_2O_3, SiC, SiO_2, TiO_2, and ZrO_2. Practically, commercial supports made of artificial materials mean expensive membranes. Therefore, many authors have focused their research on developing low-cost supports made of natural raw materials such as clay, kaolin quartz, and diatomite [20–22]. Among them, diatomite has gained a particular interest because of its unique characteristics. Diatomite is a sedimentary rock consisting of fossilized diatoms residues of hard-shelled algae type; it is a porous silicate material. They are characterized by very high porosity, high permeability, low thermal conductivity, high specific surface area, good adsorption capacity, and chemical inertness [22–24]. Diatomite is used as a filter aid, liquids absorbent, reinforcing filler in plastics and rubber, as porous medium for thermal insulation, and a good chemical catalyst [23,24]. However, only little research work has focused on the use of diatomite in the manufacture of porous ceramic membrane supports [17,25–27]. To date, no comprehensive studies on the use of porous tubular membrane supports made with diatomite and alumina mixtures have been published.

In the present study, fabrication and characterization of porous ceramic supports are reported. In order to minimize membrane costs and allow to use of our natural resources optimally, supports have been prepared from local diatomite. The choice of these materials has been driven by their natural abundance and their thermal stability. Therefore, this work aims to exploit the physical and chemical properties of natural diatomite material to develop a good quality and cost-effective ceramic membrane supports.

Materials and methods

Starting materials

Two mineral powders: Natural diatomite and alumina (Al_2O_3) were selected for the elaboration of our ceramic membrane supports. Alumina Al_2O_3 was obtained from Sigma–Aldrich; diatomite originates from the Sig region (Algeria). Alumina is intended to improve the mechanical properties of the

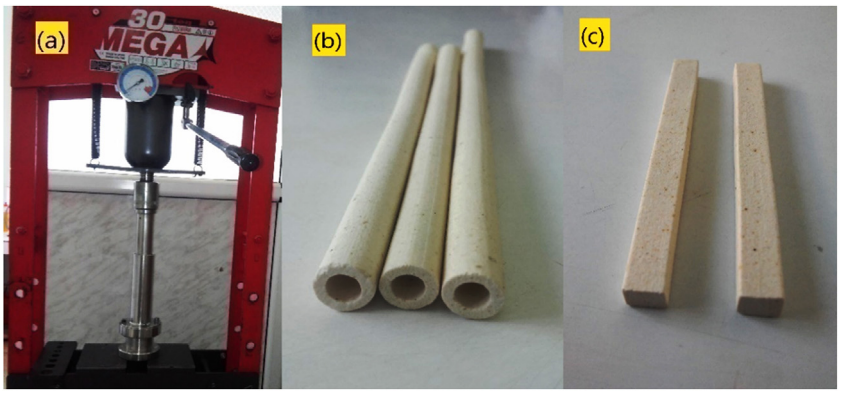

Fig. 1 – (a) A photograph of a mechanical extruder. (b, c) A photograph of prepared tubular and flat rectangular supports, respectively.

diatomite-based membrane supports. It is also used to increase the average pore size of samples. The organic additive, Methylcellulose, is used as a binder in order to improve the rheological properties of the paste; thus, it facilitates the forming of supports.

Preparation of membrane supports using extrusion method

Specimens were prepared in steps. The first step is to prepare the paste by mixing diatomite as major raw material and different amounts of alumina powders. Five different compositions were prepared by changing the relative amount of alumina (from 0 to 20 wt%) as ratios of: 100:0, 95:5, 90:10 and 80:20 (by weight). These are named: 0A, 5A, 10A and 20A, respectively. The starting materials were initially mixed with 4 wt.% methyl-cellulose as a binder. With the progressive addition of water, the powder mixture was aged to obtain a plastic paste with high homogeneity and to allow forming. Water was added to the mixtures between 35% and 40 wt.% to obtain a plastic paste that has high homogeneity and moisture content. The second step is the synthesis of membrane supports using the extrusion method (Fig. 1a). The paste was molded into two forms, tubular and flat rectangular. The flat rectangular samples have been used for mechanical tests (three-point bending test). To obtain homogeneity and quality drying, we cut the tubular supports to the desired lengths at the end of the extruder nozzle and placed them on aluminum rollers rotating evenly so that the tubes do not deform. The tubular supports have 6 mm inner and 10 mm outer diameters, while the length is selected according to our needs. After drying at room temperature, the supports (Fig. 1b, c) were sintered at temperatures ranging from 1100 to 1250 °C for 1 h. First, 2 °C/min heating rate is applied in the range 30–250 °C; then, the heating rate is increased to 5 °C/min from 250 °C to target.

Experimental procedures

Several techniques were used to investigate the proprieties of ceramic supports. The structural proprieties of the raw and supports materials were determined by X-ray diffraction (XRD) using an ULTIMA IV Rugaku, $Cu_{K\alpha}$ ($\lambda = 1.54093$ Å). The flexural strength of sintered supports has been measured by mechanical experiments consisting of a three-point standard test (five test specimens were used). The morphology and surface quality of supports were examined with scanning electron microscopy (SEM). The pore characteristics: total porosity ratio, APS or diameter, and pore size distribution (PSD) has been determined by mercury intrusion porosimetry technique (Micromeritics, Model Autopore 9220) for specimens sintered at different temperatures. Chemical analysis of raw materials was carried out by means of a Spectro iQ II X-Lab apparatus. Differential scanning calorimetry (DSC) and thermogravimetric analysis (TGA) were performed using an SDT Q600 TA Instruments from 30 to 1250 °C at a heating rate of 10 °C/min. The Fourier Transform Infrared (FT-IR) spectra are recorded in the wavenumber range between 400 and 4000 cm^{-1} at room temperature.

Results and discussion

Analysis of the raw materials

The chemical composition of the starting powders is given in Table 1 as weight percentages of oxides. It can be said that the diatomite powder is essentially composed of large amounts of silica (SiO_2) and CaO, whereas Al_2O_3, MgO, and Fe_2O_3 can be considered as impurities. The quantitative analysis of added alumina (Al_2O_3) shows that the purity of this raw material is about 99%. It also contains 0.24 wt% MgO, 0.22 wt% P_2O_5, and 0.11 wt% Na_2O as impurities. XRD patterns of the raw diatomite, calcined diatomite, and alumina powder are given in Fig. 2. The main phases forming the raw diatomite are found to be amorphous SiO_2, quartz form of SiO_2, calcite ($CaCO_3$), and ankerite ($Ca(Mg,Fe)(CO_3)_2$) (dolomite forms) (Fig. 2a) [28–30]. Fig. 2b shows that upon calcination at 800 °C for 1 h, an increase in the intensity of the quartz peak, the disappearance of the $CaCO_3$ and ankerite phases, and the appearance of wollastonite $CaSiO_3$ phase can be observed. The XRD spectrum of alumina powder involving only Al_2O_3 peaks is shown in Fig. 2c. This spectrum also shows that the alumina powder is well-crystallized.

Table 1 – Chemical composition of starting materials expressed as weight percentages for the different oxides, using the X-ray fluorescence technique.

	SiO_2	CaO	MgO	Al_2O_3	MnO	TiO_2	K_2O	Fe_2O_3	P_2O_5	CuO	Cl	Na_2O
Raw diatomite	81.98	12.63	0.99	2.46	0.02	0.03	0.10	1.19	0.30	0.04	0.17	0.11
Alumina	–	0.02	0.24	99.44	0.03	–	–	0.01	0.22	0.02	–	0.11

Table 2 – The band vibrations of the FTIR spectrum of diatomite.

V (cm^{-1})	3389	1637	1431	1068	876	798	727
Chemical bands	O—H	O—H	CO_3^{2-}	Si—O—Si	CO_3^{2-}	Si—O	CO_3^{2-}
References	[28]	[28]	[28,29]	[4,28]	[28,29]	[4,28]	[29]

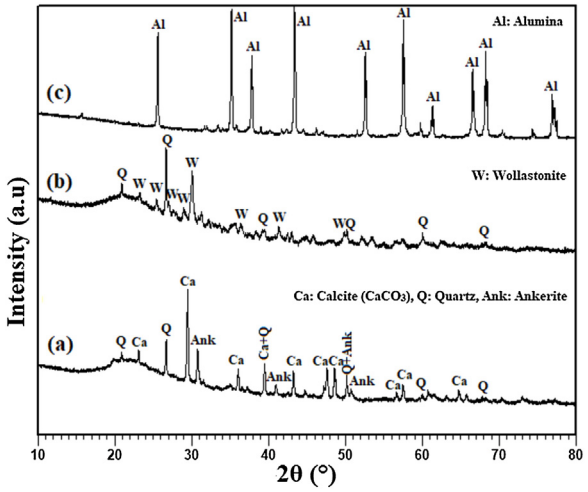

Fig. 2 – XRD spectra of (a) raw diatomite. (b) Calcined diatomite at 800 °C for 1 h. (c) Alumina powder.

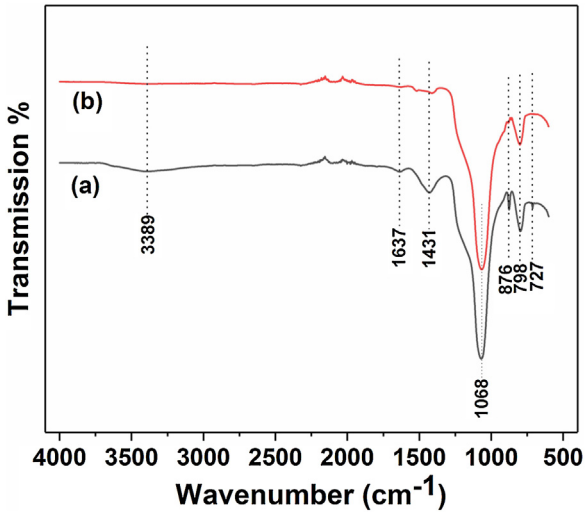

Fig. 3 – FTIR spectrum of diatomite. (a) Before and (b) after calcination at 800 °C for 1 h.

Fig. 3 and Table 2 illustrate the FTIR spectroscopy of the starting raw and calcined diatomite. The spectrum confirms the presence of CO_3^{2-} deformation bands at 1431, 876, and at 727 cm^{-1} from calcite and ankerite in diatomite. The signals

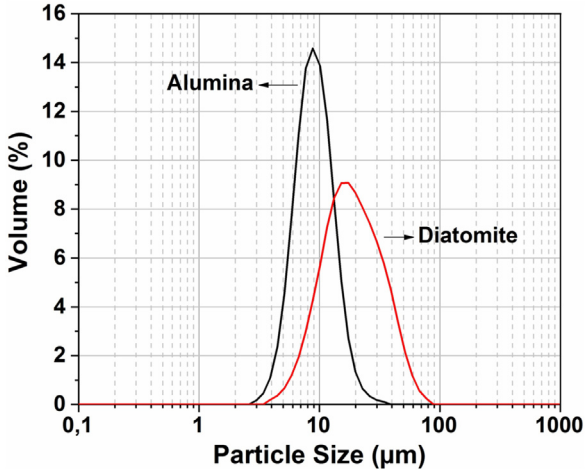

Fig. 4 – Particle size distribution for diatomite and alumina powders.

related to silica are found at 798 $cm^{-1}$and 1068 cm^{-1}. A large band centered on 3389 cm^{-1}, and the peak at 1637 cm^{-1} are attributed to the stretching and bending vibrations of O—H bond of the adsorption water; they disappear after calcination. This result indicates the hydrophilic character of raw diatomite. We can also see that the vibration CO_3^{2-} bands, initially present on the raw diatomite spectrum, disappear in the case of treated diatomite. This finding is in good agreement with the XRD results.

The particle size distribution for the raw material was measured by the Horiba laser scattering particle size distribution analyzer LA 960 (Fig. 4). This figure shows that almost 50% of the particles have a diameter below 20 μm. The average particle size for alumina and crushed diatomite is about 9 μm and 20 μm, respectively. Scanning Electron Microscopy (SEM) images of the powders are shown in Fig. 5. The raw diatomite powder consists of particles of various forms such as discs, pinnate and tubular shapes (Fig. 5a). In addition, diatomite has a porous microstructure, and some large particles are an agglomeration of smaller particles. Fig. 5b shows that the alumina particles have irregular shapes and variable sizes; plate-like particles are also present.

Differential scanning calorimetry (DSC) and thermogravimetric analysis (TGA) were used to determine the structural evolution of the raw diatomite powder (Fig. 6). These two analyses were performed under air in the range of 30–1250 °C. Fig. 6 shows the results for raw diatomite; three endothermic

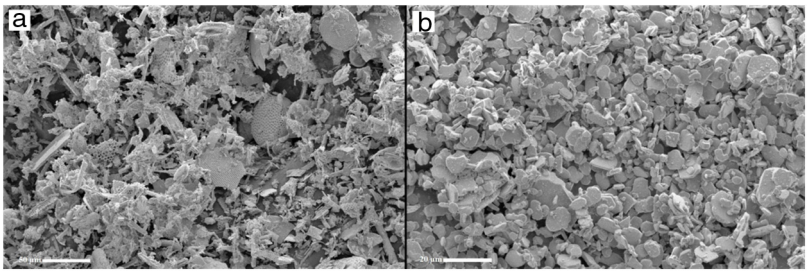

Fig. 5 – SEM micrograph of powders; (a) diatomite, (b) alumina.

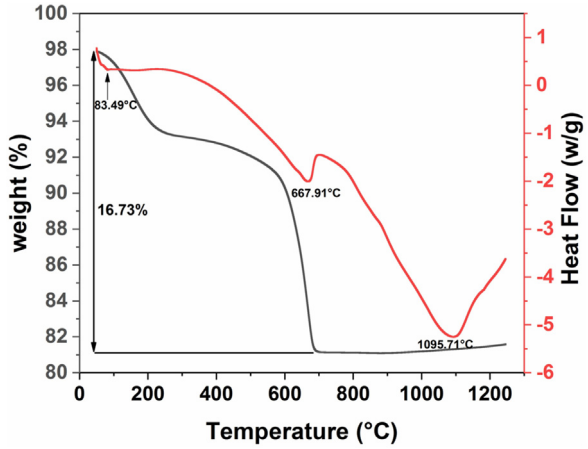

Fig. 6 – DSC and TGA curves for diatomite powder.

peaks show up on the DSC curve. The thermogravimetric curve indicates that the first and second endothermic processes are accompanied by a decrease in the mass of the sample. The first peak at about 83 °C, associated with a weight loss of about 4.4%, can be explained by the release of surface adsorbed water. The second endothermic peak at about 668 °C can be associated with a weight loss of around 12% that could be attributed to the decarbonation of calcite from ($CaCO_3$) to CaO (breakdown of carbonates accompanied by CO_2 release). The endothermic reaction, at around 1096 °C, could be caused by the transformation of the quartz to cristobalite [31].

Effect of alumina addition on the phase composition of products

Phases identification is of great importance to understand our prepared prototype and determine the application. The presence of certain phases may limit their use to the filtration of solutions. We have used XRD to investigate the influence of alumina additives on formed phases. Fig. 7 shows the XRD pattern of the samples sintered at 1200 °C for 1 h. The principal observed phases are cristobalite (tetragonal SiO_2), quartz (hexagonal SiO_2), alumina Al_2O_3, wollastonite ($CaSiO_3$), and anorthite ($CaAl_2Si_2O_8$). The cristobalite phase should be ascribed to the transformation of the amorphous silica phase ($SiO_2{\cdot}nH_2O$) into cristobalite, as well as part of quartz [31]. In all studied samples, the amorphous silica phase ($SiO_2{\cdot}nH_2O$) transformed into cristobalite rather than other silica phases during calcination, primarily because the amorphous phase was the aggregation of cristobalite microcrystalline. Quartz in raw diatomite is inclined to turn into cristobalite upon calcination rather than tridymite because of the presence of the crystal nuclei of cristobalite produced from the phase transfer of micro-amorphous silica to cristobalite; it is thought that this process lowers the activation energy [31]. For the specimens containing 20 wt.% of alumina, the latter reacts with CaO and SiO_2 to produce an anorthite phase ($CaO{\cdot}Al_2O_3{\cdot}2SiO_2$); the wollastonite phase also disappears at this percentage, and anorthite becomes more crystallized. By contrast, when supports are prepared only from diatomite, the main phases observed are wollastonite, quartz, and cristobalite.

Pore characterization for supports

For the fabrication of high-quality membrane supports, the important properties to be optimized are porosity, APS, pore size distribution, mechanical properties, chemical stability, and concentration of surface and volume defects. The open cell porosity and the APS for supports sintered at 1200 °C for 1 h, as a function of wt.% of added alumina, are illustrated in Fig. 8. The findings suggest that the average values of our quantities vary significantly and depend on the wt.% of the alumina additive. The APS gradient presents a trend dissimilar to that of the open porosity (Fig. 8a). It is clear that the alumina additive decreases the open porosity while it increases the APS. SEM micrographs confirm this result presented in Fig. 10. For example, the support (0 wt.% Alumina) has an APS around 3.3 μm and an open porosity ratio of 56%. In contrast, the support (diatomite +20 wt.% Alumina) has an APS around 20.7 μm and an open porosity ratio of 39.5%. We have to bear in mind that these supports have been sintered in the same conditions (1200 °C for 1 h). The low open porosity for samples 10A and 20A sintered at 1200 °C can be explained by the liquid phase formation following the reaction between wollastonite–silica– and anorthite. In general, the melted phase of the mixture plays a major role; it makes the material bulk denser. Alumina and impurities like CaO, MgO, K_2O, and Na_2O (Table 1) facilitate the formation of low-temperature eutectics in diatomite. Hence, we have the formation of a melt phase in silica-rich grains resulting in enlarged pores [32,33]. Fig. 8b illustrates the pore size distribution curves for supports containing 0, 5, 10, and 20 wt.% of alumina additives sintered at 1200 °C. This figure shows that for specimens prepared from diatomite alone, most of the pores have a diameter that ranges from 1.4 μm to 6 μm. whereas, for samples with alumina addition, most pores diameter ranges from 1.4 to 45 μm. This means that

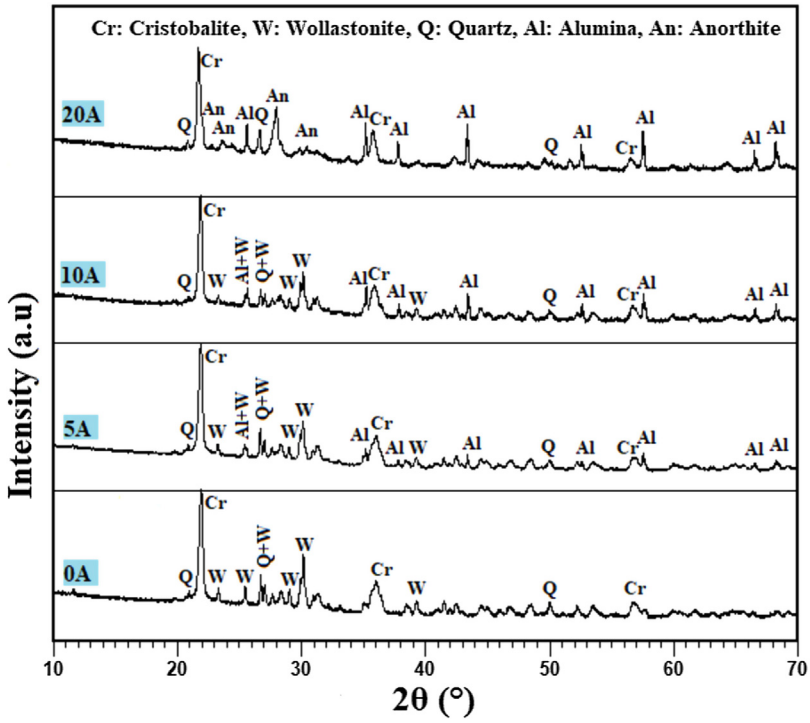

Fig. 7 – XRD spectra of support samples sintered at 1200 °C for 1 h.

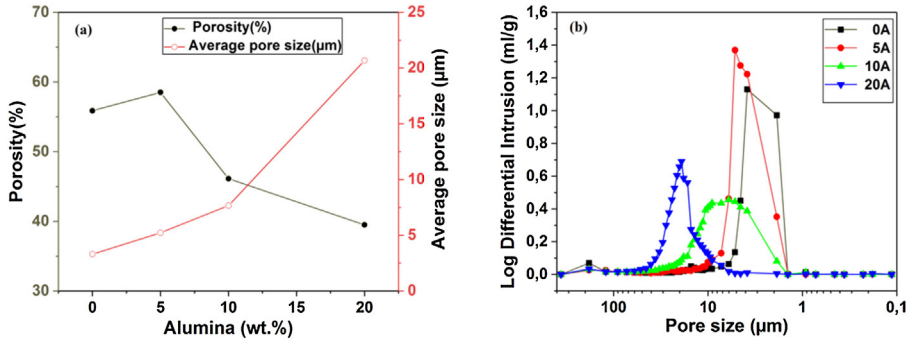

Fig. 8 – (a) Variation of average pore size and open porosity as a function of the alumina content for supports sintered at 1200 °C. (b) Pore size distribution in supports sintered at 1200 °C for 1 h.

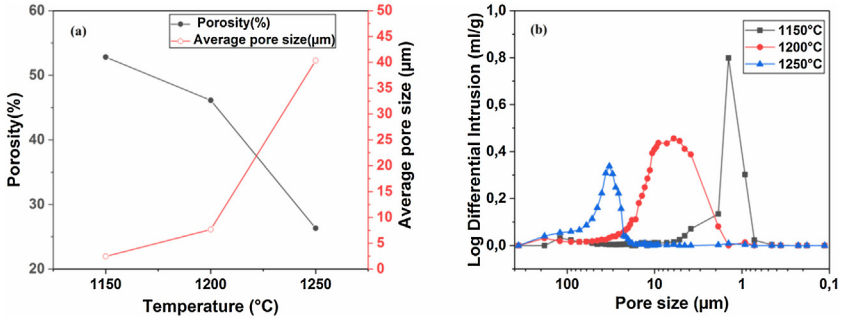

Fig. 9 – (a) Variation of average pore size and open porosity with sintering temperature for supports (10 wt.%). (b) Pore size distribution for supports (10 wt.%) sintered at different temperatures.

the APS is larger for supports prepared with alumina addition. The pore size distribution, the APS, and open porosity percentage curves for specimens containing 10 wt.% of alumina as a function of sintering temperature (1150–1250 °C) are shown in Fig. 9. This composition was chosen because it has the best characteristics in terms of the APS, the open porosity, and the flexural mechanical strength. It can be seen that APS increases with temperature, while we see the opposite

Table 3 – Some properties of samples prepared from diatomite and diatomite + alumina.

Sintering temperature (°C)	Alumina (wt.%)	Porosity (%)	Average pore size (μm)	Flexural strength (MPa)	Water permeability ($m^3/(h\,m^2\,bar)$)
1150	10	52.81	2.45	–	–
1200	0	55.88	3.30	10.57	7.99
	5	58.51	5.22	13.41	9.97
	10	46.12	7.66	28.34	15.66
	20	39.50	20.68	8.25	28.07
1250	10	26.32	40.35	–	–

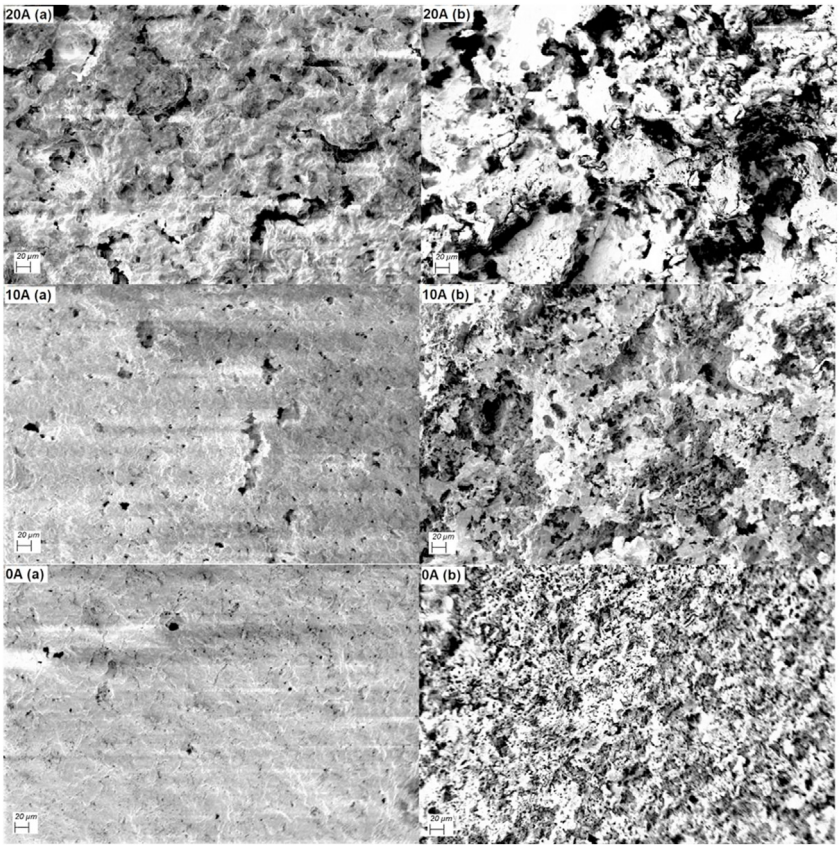

Fig. 10 – SEM micrographs of membranes support sintered at 1200 °C for 1 h. (a) Surface (b) cross-section.

for open porosity. When the sintering temperature increased from 1150 to 1250 °C, the APS moves from 2.5 to 40.4 μm while the open porosity decrease from 52.8 to 26.3%. Therefore, the ideal temperature for sintering is 1200 °C. The results above prove that the APS and the porosity can be controlled by choosing the appropriate percentage of alumina added. Structural characteristics of the final membrane supports, prepared from diatomite and alumina, are summarized in Table 3.

Supports morphology

A typical description of the microstructure of samples 0A, 10A, and 20A sintered at 1200 °C is shown in Fig. 10. This micrograph illustrates the type of pore size distribution within the matrix. Small voids are found in the microstructure of sample 0A. There are less open porosity and larger pore sizes in the microstructure of samples 10A and 20A; this is because the alumina addition helps to ease the grain growth, thus encouraging the coalescence of pores, which in turn leads to larger average pore size. In fact, the eutectic liquid phase between alumina and elements composing diatomite promotes grain growth and diffusion at around 1200 °C and also causes the enlargement of pores.

Mechanical properties

Fig. 11 presents the flexural strength of specimens sintered at 1200 °C as a function of added alumina (wt.%). Two separate stages can be noticed. First, as alumina is added, the flexural strength increases suddenly, up to 28 MPa for supports 10A, before it starts decreasing in the second stage when the content of alumina exceeds 10 wt.%. The initial increase in strength may be closely related to the effect of sintering which causes grains to densify. Sintering is a controlling factor

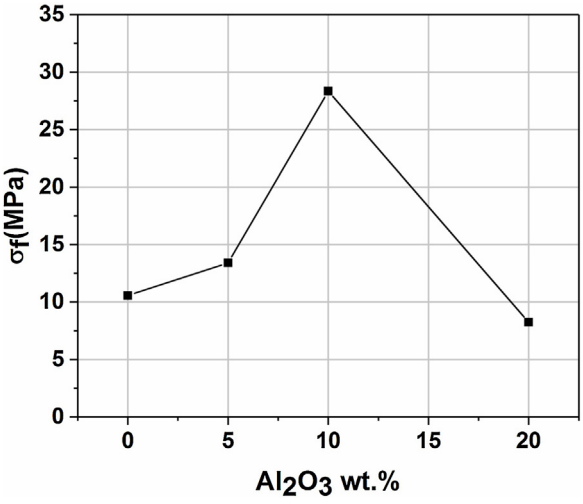

Fig. 11 – Flexural strength as a function of the alumina content for membrane supports sintered at 1200 °C for 1 h.

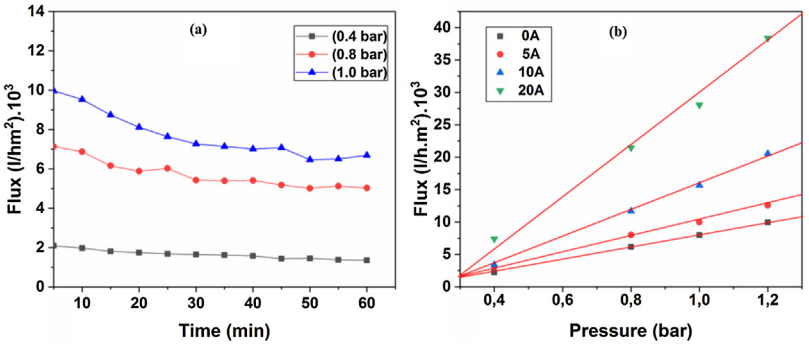

Fig. 12 – (a) Distilled water flux versus time, at different working pressures, for supports (10 wt.%) sintered at 1200 °C. (b) Water flux variation as a function of different applied pressures.

that can boost mechanical properties. However, when 20 wt.% of alumina are added, the strength value decreased sharply down to 8 MPa. Accordingly, it can be said that the flexural strength is controlled by the alumina content and sintering. Open porosity and pore size have been found to correlate with the strength of a material. As expected, samples with high open porosity (i.e. samples with 0 and 5 wt. % of Al_2O_3) and large pore size (i.e. samples with 20 wt. of Al_2O_3) have the lowest flexural strength.

Water permeability

Tangential filtration experiments were performed on prepared membrane supports, using a home-made pilot plant at room temperature. Fig. 12a shows water permeability through the support (10% sintered at 1200 °C) measured as a function of time and applied pressure. A stable flux is obtained after 30 min. Correspondingly, the flux increases with the applied pressure; this is because the pressure enhances the convective driving force in the membrane support [34,35]. Additionally, the effect of the applied pressure on water permeates flux has been taken into account. Fig. 12b shows the flux of distilled water through the supports 0, 5, 10, and 20A as a function of applied pressure. As can be seen in Fig. 12b, with an increasing applied pressure difference (from 0.4 to 1.2 bar), the flux increases linearly for all samples; this indicates that the pressure difference is the only driving force for permeation. The average permeability values are 8, 10, 15, and 28 $m^3\,h^{-1}\,m^{-2}\,bar^{-1}$ for supports 0A, 5A, 10A and 20A, respectively. This trend is due to the effect of larger pore size that causes the increases in water flux. Because of the lower average pore size (≈3 μm), the flux of water permeability is found to be relatively low, as expected for support 0A. Another fact is that the water flux increases proportionally with the added alumina. The porosimetry characterization results indicate that the APS varies exponentially with the amount of alumina added. We must remember, also, that the most important factor affecting the flux and permeability is the pore size, as can be demonstrated by the Hagen–Poiseuille equation [36].

Conclusions

In this study, novel porous ceramic supports were fabricated with a wide range of average pore sizes (2.5–40.4 μm), total open porosity (26.3–58.5%), and pore size distributions. It has been observed that the supports prepared by adjusting the percentage of added alumina and the sintering temperature can have promised physical properties. Under identical conditions, alumina additions may enhance both the mechanical

proprieties and pore size. However, the effect of Al_2O_3 on porosity is harmful. The APS increases as the concentration of alumina increases. Good mechanical properties are obtained by the addition of 10 wt.% of alumina, while permeability significantly improves from 8 to 15. The results show that the best features of supports are obtained with the addition of 10 wt. % of alumina and with a sintering temperature around 1200 °C for 1 h. It is evident from this work that the substrate can be used as a support for microfiltration or ultrafiltration. Indeed, diatomite and alumina enhance mechanical properties and thus maintain the integrity of the porous membranes and provide excellent water permeability.

REFERENCES

[1] E. Nazarova, D.S. Alimova, V.I. Mikhaylov, E.F. Krivoshapkina, P.V. Krivoshapkin, Macroporous ceramic filters from mineral raw materials for machine oils filtration, Ceram. Int. 45 (2019) 8767–8773, http://dx.doi.org/10.1016/j.ceramint.2019.01.201.

[2] N. Malik, V.K. Bulasara, S. Basu, Preparation of novel porous ceramic microfiltration membranes from fly ash, kaolin and dolomite mixtures, Ceram. Int. 46 (5) (2020) 6889–6898, http://dx.doi.org/10.1016/j.ceramint.2019.11.184.

[3] A. Boulkrinat, F. Bouzerara, A. Harabi, K. Harrouche, S. Stelitano, F. Russo, F. Galiano, A. Figoli, Synthesis and characterization of ultrafiltration ceramic membranes used in the separation of macromolecular proteins, J. Eur. Ceram. Soc. 40 (2020) 5967–5973, http://dx.doi.org/10.1016/j.jeurceramsoc.2020.06.060.

[4] S. Benayache, S. Alleg, A. Mebrek, J.J. Suñol, Thermal and microstructural properties of paraffin/diatomite composite, Vacuum 157 (2018) 136–144, http://dx.doi.org/10.1016/j.vacuum.2018.08.044.

[5] A. Harabi, N. Karboua, S. Achour, Effect of thickness and orientation of alumina fibrous thermal insulation on microwave heating in a modified domestic 2.45 GHz multi-mode cavity, Int. J. Appl. Ceram. Technol. 9 (2012) 124–132, http://dx.doi.org/10.1111/j.1744-7402.2011.02632.x.

[6] F. Bouzerara, S. Boulanacer, A. Harabi, Shaping of microfiltration (MF) ZrO_2 membranes using a centrifugal casting method, Ceram. Int. 41 (2015) 5159–5163, http://dx.doi.org/10.1016/j.ceramint.2014.11.141.

[7] N. medjemem, A. Harabi, F. Bouzerara, L. Foughali, B. Boudaira, A. Guechi, N. Brihi, Elaboration and characterization of low-cost ceramics microfiltration membranes applied to the sterilization of plant tissue culture media, J. Taiwan Inst. Chem. Eng. 59 (2016) 79–85, http://dx.doi.org/10.1016/j.jtice.2015.07.032.

[8] S.T. Kassa, C.C. Hu, Y.C. Liao, J.K. Chen, J.P. Chu, Thin film metallic glass as an effective coating for enhancing oil/water separation of electrospun polyacrylonitrile membrane, Surf. Coat. Technol. 368 (2019) 33–41, http://dx.doi.org/10.1016/j.surfcoat.2019.04.030.

[9] B. Zhu, M. Duke, L.F. Dumee, A. Merenda, E. des Ligneris, L. Kong, P.D. Hodgson, S. Gray, Short review on porous metal membranes-fabrication, commercial products, and applications, Membranes (Basel) 8 (2018) 83, http://dx.doi.org/10.3390/membranes8030083.

[10] D.Z. Sun, X. Duan, W. Li, D. Zhou, Demulsification of water-in-oil emulsion by using porous glass membrane, J. Memb. Sci. 146 (1998) 65–72, http://dx.doi.org/10.1016/S0376-7388(98)00096-9.

[11] J.H. Ha, S.Z.A. Bukhari, J. Lee, I.H. Song, Preparation and characterisation of aluminabased composite support layers, Adv. Appl. Ceram. 115 (2016) 229–235, http://dx.doi.org/10.1080/17436753.2015.1126953.

[12] D. Liang, J. Huang, H. Zhang, H. Fu, Y. Zhang, H. Chen, Influencing factors on the performance of tubular ceramic membrane supports prepared by extrusion, Ceram. Int. (2021), http://dx.doi.org/10.1016/j.ceramint.2020.12.235.

[13] J. Wehling, J. Köser, P. Lindner, C. Lüder, S. Beutel, S. Kroll, K. Rezwan, Silver nanoparticle-doped zirconia capillaries for enhanced bacterial filtration, Mater. Sci. Eng. C 48 (2015) 179–187, http://dx.doi.org/10.1016/j.msec.2014.12.001.

[14] A. Abdullayev, M.F. Bekheet, D.A.H. Hanaor, A. Gurlo, Materials and applications for low-cost ceramic membranes, Membranes (Basel) 9 (2019) 1–32, http://dx.doi.org/10.3390/membranes9090105.

[15] D. Vasanth, G. Pugazhenthi, R. Uppaluri, Fabrication and properties of low-cost ceramic microfiltration membranes for separation of oil and bacteria from its solution, J. Memb. Sci. 379 (2011) 154–163, http://dx.doi.org/10.1016/j.memsci.2011.05.050.

[16] M. Issaoui, L. Limousy, Low-cost ceramic membranes: synthesis, classifications, and applications, Comptes Rendus Chim. 22 (2019) 175–187, http://dx.doi.org/10.1016/j.crci.2018.09.014.

[17] P.V. Vasconcelos, J.A. Labrincha, J.M.F. Ferreira, Permeability of diatomite layers processed by different colloidal techniques, J. Eur. Ceram. Soc. 20 (2000) 201–207, http://dx.doi.org/10.1016/S0955-2219(99)00139-9.

[18] J.H. Ha, J. Lee, I.H. Song, The preparation and characterizations of the diatomite-kaolin composite support layer for microfiltration, J. Ceram. Soc. Jpn. 123 (2015) 656–661, http://dx.doi.org/10.2109/jcersj2.123.656.

[19] B.K. Nandi, R. Uppaluri, M.K. Purkait, Preparation and characterization of low-cost ceramic membranes for micro-filtration applications, Appl. Clay Sci. 42 (2008) 102–110, http://dx.doi.org/10.1016/j.clay.2007.12.001.

[20] C. Kadiri, A. Harabi, F. Bouzerara, L. Foughali, N. Brihi, S. Hallour, A. Guechi, B. Boudaira, Preparation and properties of tubular macroporous ceramic membrane supports based on natural quartz sand and dolomite, J. Aust. Ceram. Soc. 56 (2020) 379–387, http://dx.doi.org/10.1007/s41779-019-00338-2.

[21] N. Kouras, A. Harabi, F. Bouzerara, L. Foughali, A. Policicchio, S. Stelitano, F. Galiano, A. Figoli, Macro-porous ceramic supports for membranes prepared from quartz sand and calcite mixtures, J. Eur. Ceram. Soc. 37 (2017) 3159–3165, http://dx.doi.org/10.1016/j.jeurceramsoc.2017.03.059.

[22] P. Monash, G. Pugazhenthi, P. Saravanan, Various fabrication methods of porous ceramic supports for membrane applications, Rev. Chem. Eng. 29 (2013) 357–383, http://dx.doi.org/10.1515/revce-2013-0006.

[23] H.E.G.M. Bakr, Diatomite: its characterization, modifications and applications, Asian J. Mater. Sci. 2 (3.) (2010) 121–136, http://dx.doi.org/10.3923/ajmskr.2010.121.136.

[24] M.M. Ghobara, A. Mohamed, Diatomite in Use: Nature, Modifications, Commercial Applications and Prospective Trends, Scrivener Publishing LLC, Beverly, CA, USA, 2019, pp. 471–509, http://dx.doi.org/10.1002/9781119370741.ch19.

[25] J.H. Ha, E. Oh, I.H. Song, The fabrication and characterization of sintered diatomite for potential microfiltration applications, Ceram. Int. 39 (2013) 7641–7648, http://dx.doi.org/10.1016/j.ceramint.2013.02.102.

[26] J.H. Ha, S. Lee, S.Z. Abbas Bukhari, J. Lee, I.H. Song, The preparation and characterization of alumina-coated pyrophyllite-diatomite composite support layers, Ceram. Int. 43 (2017) 1536–1542, http://dx.doi.org/10.1016/j.ceramint.2016.10.127.

[27] J.H. Ha, D.W. Jung, I.H. Song, The effect of an alumina coating on the pore characteristics of a diatomite-kaolin composite support layer, Ceram. Int. 40 (2014) 12961–12967, http://dx.doi.org/10.1016/j.ceramint.2014.04.157.

[28] T. Benkacem, B. Hamdi, A. Chamayou, H. Balard, R. Calvet, Physicochemical characterization of a diatomaceous upon an acid treatment: a focus on surface properties by inverse gas chromatography, Powder Technol. 294 (2016) 498–507, http://dx.doi.org/10.1016/j.powtec.2016.03.006.
[29] H. Hadjar, B. Hamdi, M. Jaber, J. Brendlé, Z. Kessaïssia, H. Balard, J.B. Donnet, Elaboration and characterisation of new mesoporous materials from diatomite and charcoal, Micropor. Mesopor. Mater. 107 (2008) 219–226, http://dx.doi.org/10.1016/j.micromeso.2007.01.053.
[30] O. Hadjadj-Aoul, R. Belabbes, M. Belkadi, M.H. Guermouche, Characterization and performances of an Algerian diatomite-based gas chromatography support, Appl. Surf. Sci. 240 (2005) 131–139, http://dx.doi.org/10.1016/j.apsusc.2004.06.108.
[31] R. Zheng, Z. Ren, H. Gao, A. Zhang, Z. Bian, Effects of calcination on silica phase transition in diatomite, J. Alloys Compd. 757 (2018) 364–371, http://dx.doi.org/10.1016/j.jallcom.2018.05.010.
[32] F. Akhtar, Y. Rehman, L. Bergström, A study of the sintering of diatomaceous earth to produce porous ceramic monoliths with bimodal porosity and high strength, Powder Technol. 201 (3) (2010) 253–257, http://dx.doi.org/10.1016/j.powtec.2010.04.004.
[33] X. Wang, J. Fuh, Y. Wong, et al., Laser sintering of silica sand-mechanism and application to sand casting mould, Int. J. Adv. Manuf. Technol. 21 (2003) 1015–1020, http://dx.doi.org/10.1007/s00170-002-1424-x.
[34] M. Mohamed Bazin, N. Ahmad, Y. Nakamura, Preparation of porous ceramic membranes from Sayong ball clay, J. Asian Ceram. Soc. 7 (2019) 417–425, http://dx.doi.org/10.1080/21870764.2019.1658339.
[35] P. Kamgang-Syapnjeu, D. Njoya, E. Kamseu, L. Cornette de Saint Cyr, A. Marcano-Zerpa, S. Balme, M. Bechelany, L. Soussan, Elaboration of a new ceramic membrane support from Cameroonian clays, coconut husks and eggshells: application for Escherichia coli bacteria retention, Appl. Clay Sci. 198 (2020) 105836, http://dx.doi.org/10.1016/j.clay.2020.105836.
[36] M. Lorente-ayza, S. Mestre, M. Menéndez, E. Sánchez, Comparison of extruded and pressed low-cost ceramic supports for microfiltration membranes, J. Eur. Ceram. Soc. 35 (2015) 3681–3691, http://dx.doi.org/10.1016/j.jeurceramsoc.2015.06.010.